



## Supporting Online Material for

### ***Chlamydomonas* Swims with Two "Gears" in a Eukaryotic Version of Run-and-Tumble Locomotion**

Marco Polin, Idan Tuval, Knut Drescher, J. P. Gollub, Raymond E. Goldstein\*

\*To whom correspondence should be addressed. E-mail: R.E.Goldstein@damtp.cam.ac.uk

Published 24 July 2009, *Science* **325**, 487 (2009)

DOI: 10.1126/science.1172667

#### **This PDF file includes:**

Materials and Methods  
Figs. S1 to S3  
References

# Supporting Online Material

## Materials and methods

### Culturing of algae

Experiments were conducted on *Chlamydomonas reinhardtii* (UTEX 89 (S1)), grown axenically in standard *Volvox* medium (SVM (S2)) with sterile air bubbling, in diurnal growth chambers (Binder KBW400, Tuttlingen, Germany) set to a daily cycle of 16 h in cool white light ( $\sim 4000$  lux) at 28° C, and 8 h in the dark at 26° C. In all experiments, the algae were harvested during the exponential growth phase ( $\lesssim 10^6$  cells/ml), to guarantee high uniformity and health of the population.

### Macroscopic diffusion experiment

For the macroscopic diffusion experiment, we used the horizontal view camera of the 3D tracking setup (described below) in darkfield. Newly harvested suspensions of *C. reinhardtii* were transferred to 1.5 ml disposable Plastibrand UV-cuvettes (Brand GmbH, Wertheim, Germany), where they filled a volume of  $\sim 20 \times 12.2 \times 4$  mm. Each sample was then sealed with an expanded polystyrene foam cork, and centrifuged at 350 g for 2.5 min, causing the sedimentation of the suspended algae. After centrifugation, the samples were transferred to the tracking setup and the upward spreading of the cells' density profile was recorded at 10 fps for 1 – 2 min. In all experiments, recording started within the first 20 s after centrifugation. The samples were illuminated by a narrowband LED with an emission peak centered at 655 nm, and a bandwidth of 21 nm. *C. reinhardtii* is insensitive to these wavelengths (S3, S4), so phototactic reorientations do not occur. After each experiment, we homogenized the suspension by vortexing and estimated the average cell density with a Neubauer haemocytometer (Fisher Scientific, Pittsburgh,

PA). All experiments were done at average densities smaller than  $2.7 \times 10^6$  cells/ml to minimize cell-cell interactions.

We also examined the possible influence of thermal convection by recording the motion of a suspension of  $1 \mu\text{m}$  polystyrene beads (F8823, Invitrogen, Carlsbad, CA) in the same cuvette and under the same observation conditions as the previous experiments. The motion of the tracer particles was analyzed with an open source Matlab PIV toolbox (MatPIV, <http://www.math.uio.no/~jks/matpiv/>) and found to be below  $13 \mu\text{m/s}$ .

### **Flagellar dynamics experiment**

Sample cells were constructed by gluing two strips of 3 mm thick expanded polystyrene foam between two microscope coverslips. Two sides of the cell were left open to allow access. For each experiment a new sample cell was filled with fresh sterile filter-cleaned SVM at room temperature. A small number of *C. reinhardtii* cells were harvested from the culturing flask during the light cycle, and immediately transferred to the sample cell. Observations started 30 min after transfer to allow for acclimatization. Individual cells were held at the end of a micropipette with a tip opening of  $2 - 4 \mu\text{m}$ , prepared with a commercial pipette puller (P-97, Sutter Instrument Co., Novato, CA) and reshaped with a microforge (DMF1000, World Precision Instruments, Sarasota, FL). Pipettes were held in a motorized micromanipulator under joystick control (PatchStar, Scientifica, Uckfield, UK) by means of pipette holders (World Precision Instruments) mounted on small custom made rotation stages. This arrangement allowed free rotation around the pipette axis, which was crucial for reorienting the cells and achieving optimal visualization of their flagella. Cells were held by gentle suction, controlled by a gas-tight syringe fitted with micrometer control (Manual Injector, Sutter). Imaging was done under brightfield illumination on a custom-built stage mounted on a Nikon TE2000-U inverted microscope with a Nikon Plan Fluor ELWD  $40\times$  objective (NA 0.6). The light from the microscope's

halogen lamp was filtered through a long pass interference filter with a 10 nm transition width between 0.001% and 80% transmittance, centered at 620 nm (Knight Optical, Harrietsham, UK). These wavelengths were selected to avoid any phototactic response (*S3, S4*). Videos were acquired at 500 fps with a high-speed video camera (Phantom V5.1, Vision Research, Wayne, NJ) with 4 Gb of on-board memory, mounted on the microscope's camera port, and transferred to disk afterwards.

### **Experiment on rotation of unflagellated cells**

During periods of asynchrony one flagellum beats faster than the other, a pattern that should naturally lead to turns in the swimming trajectory. We reasoned that the turning rate induced by the faster flagellum could be estimated from the turning rate of a cell with a single flagellum. PVC O-rings 2 mm thick and 1 cm in diameter were fixed on the surface of microscope coverslips coated with a  $\sim 200 \mu\text{m}$  thick layer of Polydimethylsiloxane (PDMS) (Sylgard 184, Dow Corning Ltd, Coventry, UK) and sealed from outside with additional PDMS to create a circular chamber open from the top. The chambers were then cured at 60° C for 90 min, plasma etched with dry air for 30 s (Femto System, Diener Electronic, Germany) and left overnight immersed in 5% bovine serum albumin (BSA) in phosphate-buffered saline solution at 4° C. This treatment minimizes sticking of *C. reinhardtii* to the bottom of the chamber (*S5*). Before each experiment, a new chamber was taken from the BSA solution, carefully washed with fresh SVM, then filled with fresh SVM at room temperature, and placed on the stage of a Nikon TE2000-U inverted microscope. For each experiment, a small sample was harvested from the *C. reinhardtii* culturing flask and gently sheared in a borosilicate Dounce homogenizer (Fisher) to create a sub-population of unflagellated algae. A small volume from the sheared suspension was then transferred to the observation chamber. The unflagellated cells are unable to swim and therefore sink to the bottom of the cell, where they start rotating in place under the action of

their only flagellum. Each batch was observed for no longer than 15 min after homogenization. We recorded the rotation of 8 randomly chosen cells for 50 s each. All observations were done under the same brightfield conditions, with the same objective, and with the same high-speed camera used for the flagellar dynamics experiment.

### **Three-dimensional tracking experiment**

To track *C. reinhardtii*, in three dimensions, a custom-built dual view apparatus was employed (S6). Previous studies in which *Chlamydomonas* has been tracked were done in 2D (S7, S8, S9) or with a 3D moving stage tracking microscope (S10). The cells were imaged from two orthogonal directions by two identical assemblies, each consisting of a long working distance microscope (InfiniVar CFM-2/S, Infinity Photo-Optical, Boulder, CO) directly attached to a grayscale FireWire CCD camera (Pike F145B, Allied Vision Technologies, Stadroda, Germany). The sample was illuminated in darkfield by red annular LED arrays (LFR-100-R, CCS Inc., Kyoto, Japan, peak emission at 655 nm, bandwidth 21 nm). Images were acquired synchronously from both cameras with custom Labview (National Instruments, Austin, TX) routines at 20 fps and at a magnification of  $0.63\times$ . A set of 2D tracks was then computed for the image sequences acquired by each camera. As the two cameras had one common axis, 3D tracks could be reconstructed by locking together two 2D tracks which overlapped in time and had a strongly correlated trajectory along the common axis. This method allowed 10 - 100 *C. reinhardtii* cells to be tracked in one image sequence with a spatial precision better than  $3\ \mu\text{m}$  at each time point. The sample, a  $1 \times 1 \times 4$  cm quartz cuvette (111-10-40, Hellma, Müllheim, Germany), was filled with *C. reinhardtii* suspended in SVM (cleaned by filtration through a  $0.2\ \mu\text{m}$  filter) at a concentration of  $\sim 10^2$  cells/ml. Measurements began 15 min after the sample was placed in the centre of a stirred water bath at  $22^\circ\text{C}$ , as control studies with  $10\ \mu\text{m}$  polystyrene microspheres (C37259, Invitrogen) showed that thermal convection ceased  $\sim 10$  min after the sample was

placed in the water bath. The apparatus was calibrated and tested as described by Drescher et al. (S6).

## Data analysis

All analyses were done with customized Matlab routines.

### Flagellar dynamics experiment

We analyzed 24 different cells and gathered individual time series lasting typically 3 min each. Each movie was processed by local background subtraction followed by light smoothing to enhance the contrast of the flagella. The cell dynamics was quantified by monitoring the passage of each flagellum across a small interrogation region on either side of the cell body (Fig. 2A), and representing the resultant oscillatory signals of the left ( $L$ ) and right ( $R$ ) flagella as  $X_{L,R}(t) = \Gamma_{L,R}(t) \sin(2\pi\theta_{L,R}(t))$ , where  $\Gamma$  is the amplitude and  $\theta$  is the phase, normalized to advance by 1 per cycle. Unfortunately we could not determine the correspondence between  $L/R$  and *cis/trans* flagella. This correlation could be important to connect our findings to phototaxis, where intrinsic differences between *cis* and *trans* flagella are thought to play a major role (S11), but it does not influence our results and was not pursued further.

For the issue of synchronization, we focus attention on the phase difference  $\Delta(t) = \theta_L(t) - \theta_R(t)$ . We define the instantaneous beating rate of the flagellum  $i$  as  $\nu_i = d\theta_i/dt$ , and thus in synchronous beating  $\Delta$  is a constant, whereas asynchronous dynamics appears as a “drifting” phase with temporal slope  $d\Delta/dt = \nu_L - \nu_R$ . We analyzed separately the dynamics of  $\Delta(t)$  during periods of synchrony and during periods of drift. While the detailed microscopic equations of motion of beating flagella have been the subject of extensive research (S12, S13), we focus instead on how the simplest mathematical model of noisy coupled oscillators can capture the basic phenomenology of the observed time series, and give insights into the underlying bio-

chemical processes. Under general conditions the dynamics of weakly nonlinear self-sustained oscillators obey a universal equation (S14) dictated by symmetries. Modifying this to include noise of the oscillators leads to a stochastic ordinary differential equation for the phase difference (S14)

$$\frac{d\Delta}{dt} = \delta\nu - 2\pi\epsilon \sin(2\pi\Delta) + \xi(t), \quad (1)$$

where  $\delta\nu = \nu_L - \nu_R$  is the difference between the intrinsic frequencies of the two flagella,  $\epsilon$  the coupling strength, and  $\xi$  is Gaussian white noise with  $\langle \xi(t) \rangle = 0$  and correlation  $\langle \xi(t)\xi(t') \rangle = 2T_{\text{eff}}\delta(t-t')$ . Here  $T_{\text{eff}}$  is an effective “temperature” by analogy with systems in thermal equilibrium. Without noise, Eq. 1 has been derived from the low Reynolds number hydrodynamic interaction between two idealized flagella (S15). This derivation yields a rough estimate  $\epsilon_m$  for the hydrodynamic contribution to the coupling as a function of the separation of the flagella. In the present case  $\epsilon_m = 0.006 \times \bar{\nu}$ , where  $\bar{\nu} = 50$  Hz is the average flagellar beating frequency. At a heuristic level, Eq. 1 also describes the noise-driven motion of a massless particle on a “tilted washboard” potential, a rich problem with broad applicability (S16, S17). Applied to *C. reinhardtii*, this model describes periods of synchrony as localized fluctuations around a single metastable minimum of the effective potential. The noise can induce occasional hopping between metastable states, representing an extra beat of one of the flagella (a “phase slip”). The intrinsic frequency difference  $\delta\nu$  corresponds to a global tilt in the washboard potential, which favors slips in one direction.

During synchronous periods, Eq. 1 predicts that fluctuations of  $\Delta(t)$  should have an exponentially decaying autocorrelation function,  $R(t) = R_0 e^{-t/\tau_{\text{ac}}}$ , which is indeed observed experimentally (Fig. S1). If the coupling strength  $2\pi\epsilon$  is sufficiently larger than the bias  $\delta\nu$ , the

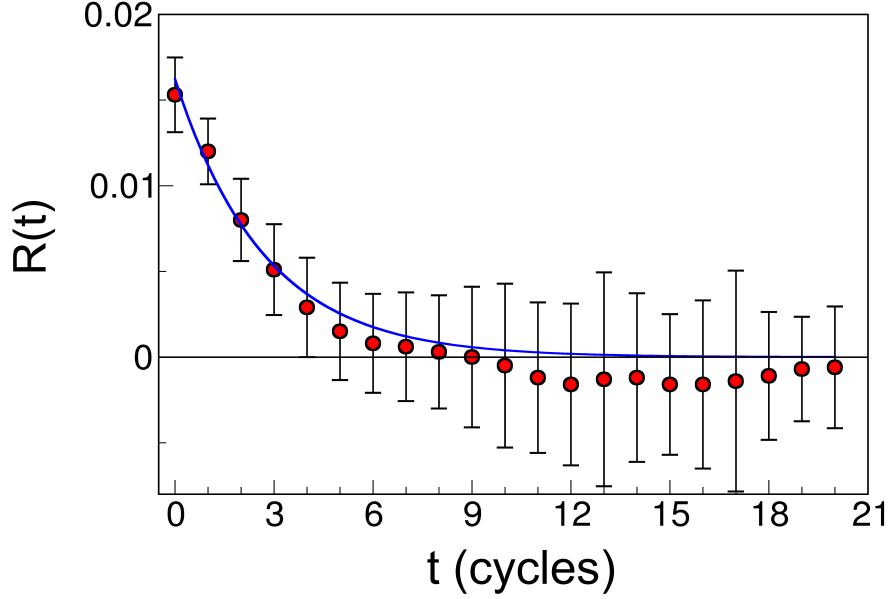


Figure S1: Average autocorrelation function  $R(t)$  in the synchronized state for one experiment, showing exponential decay with a characteristic time of  $\simeq 2$  cycles. Errorbars represent the standard deviations of the distributions used to calculate the averages.

parameters of the autocorrelation function can be expressed as

$$R_0 = \tau_{ac} T_{eff} \quad ; \quad \tau_{ac} = \frac{1}{2\pi\sqrt{(2\pi\epsilon)^2 - \delta\nu^2}}. \quad (2)$$

Following Eq. 1, we can also express the ratio  $p_+/p_-$  between the probabilities of forward and backward slips as

$$p_+/p_- = \exp(\delta\nu/T_{eff}). \quad (3)$$

Experimentally, this quantity can be estimated as the ratio between the number of positive and negative slips. We used Eqs. 2 and 3 to derive the parameters representing the synchronous dynamics of each experiment. The results ( $2\pi\epsilon \simeq 10 \delta\nu$ ) justify the use of the approximate relations in Eq. 2. These parameters are also consistent with independent observables like the

small interflagellar phase lag during synchrony reported in previous studies ( $\simeq 1/11$ th of a cycle, (S18)), and the average time between successive slips. During drift periods  $\Delta(t)$  depends linearly on time with a slope given by the bias,  $\delta\nu$ . Fluctuations around this linear behavior provide a direct measurement of the effective temperature  $T_{\text{eff}}$ . In this regime, the coupling strength is much smaller than the bias, and cannot be estimated.

For the purposes of presentation, the fitted parameters  $\delta\nu$ ,  $\epsilon$ , and  $T_{\text{eff}}$  are rescaled by the mean observed flagellar beating frequency  $\bar{\nu}$ . For the synchronous intervals, the distribution of the measured coupling parameter  $\epsilon/\bar{\nu}$  (Fig. 3A) shows a well-defined peak at a value of 0.0076, which compares very well with the rough estimate  $\epsilon_m/\bar{\nu} = 0.006$  given by the idealized flagellar model with hydrodynamic coupling (S15). The synchronous and asynchronous states cluster into two distinct regions in the parameter space  $(\delta\nu, T_{\text{eff}})$  (Fig. 3B). Synchronous states have  $\delta\nu/\bar{\nu} \simeq 0.001 - 0.01$ , while asynchronous states display  $\delta\nu/\bar{\nu} \simeq 0.1 - 0.4$ . The latter is in agreement with the asynchronous characteristics reported in earlier work (S18, S19, S20). We never observed any cell whose frequency difference falls in between these two clusters.

### **Experiment on rotation of unflagellated cells**

Recorded movies were processed as reported in the previous section. We measured the rotation speed of the cell bodies using the signal from a single interrogation region inside the body's image. At the same time, the beating frequency of the flagellum was measured from its passage across a ring-shaped interrogation area around the cell body. As this estimate neglects the drag produced by the second flagellum it provides an upper bound on the possible angular speeds. The ratio between the body's mean angular velocity and the beating frequency of the flagellum gives the angular deviation per beat. From 8 cells we obtain an average rotation rate  $\phi = 0.43 \pm 0.06$  rad/beat, consistent with an earlier observation of cell rotation by a single active flagellum after a photoshock response (S21). In low Reynolds number flow, this value is

independent of flagellar beating frequency and depends only on the geometry of the beat. From the observed difference in flagellar beating frequencies during drifts,  $\delta\nu = 5 - 15$  Hz, we obtain the two-dimensional angular speed  $\Omega_{2D} = \phi \delta\nu \simeq 2 - 6$  rad/s.

This simple derivation neglects the influence of the nearby wall on the cell body’s drag coefficient. However, since the cell’s angular velocity is perpendicular to the wall, this effect is negligible (S22), and the previous measurements give a sound estimate of the angular velocity  $\Omega_{2D}$  that a cell would have during drift periods, if its motion was planar. This is an upper bound, as the helical progression of free swimming cells tends to average out the effect of a constant frequency difference between the two flagella. A more accurate estimate can be derived if we model a cell freely swimming in the laboratory frame of reference, as simply spinning at a constant speed  $\omega$  around its own body axis. During periods of drift, this axis rotates at an angular speed  $\Omega_{2D}$  around an axis fixed in the body frame. The resulting maximum angular speed of the body axis in the laboratory frame,  $\Omega_{3D}$ , can be readily calculated. For  $\omega = 2\pi - 4\pi$  rad/s (S18) and  $\Omega_{2D} = 2 - 6$  rad/s, we obtain  $\Omega_{3D} = 0.1 - 0.7 \times \Omega_{2D} \simeq 0.8 - 2.4$  rad/s compatible with the range of maximum angular speeds obtained from 3D tracks.

### **Tracking experiment**

From the three-dimensional tracks, the angular speed  $\Omega$  between timesteps  $i$  and  $i + 1$  was computed by multiplying the frame rate (20 fps) by the angle between the normalized velocity vectors  $\hat{\mathbf{v}}_i$ , and  $\hat{\mathbf{v}}_{i+1}$ . To reduce noise, and the effect of the swimming helix, the velocity vector  $\hat{\mathbf{v}}_j$  was computed by fitting a second order polynomial to time series of  $x$ ,  $y$ , and  $z$  that contain 51 positions (from  $j - 25$  to  $j + 25$ ) and differentiating this fit at time  $j$ . This procedure yields a time series  $\Omega(t)$  that retains a background signal  $\lesssim 0.3$  rad/s, and occasional large peaks. We identified peaks to be “large peaks”, when the local maximum of the peak,  $\Omega_{\text{peak}}$ , was larger than the preceding and succeeding local minima by 0.5 rad/s. This threshold was verified by

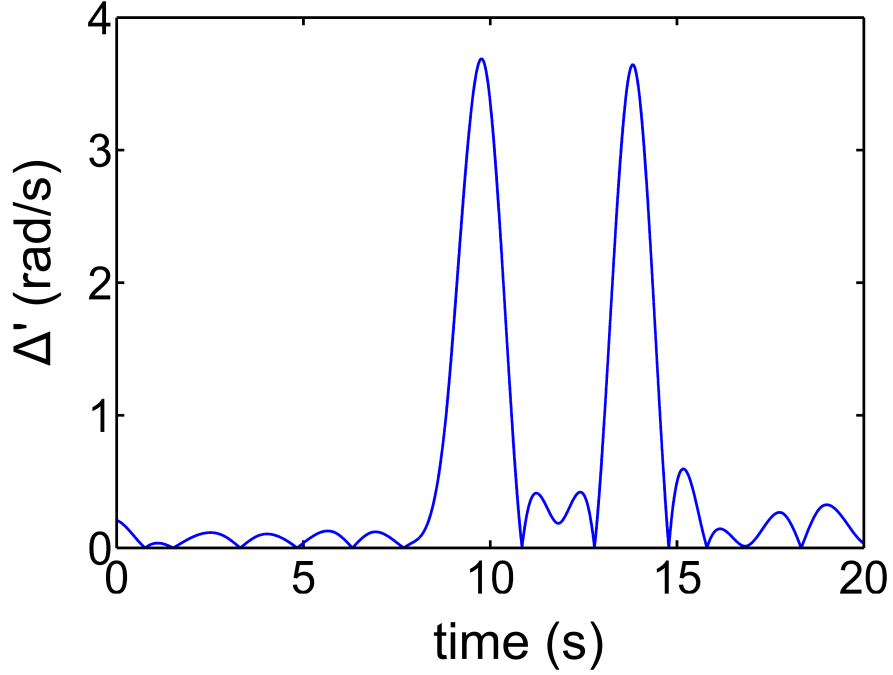


Figure S2: Time derivative  $\Delta'(t)$  of the smoothed interflagellar phase difference shows two clear peaks corresponding to two periods of phase drift. The width of the peaks measures the duration of the drifts.

checking that the large peaks in  $\Omega(t)$  correspond to obvious large-angle turns in the 3D tracks. We estimated the duration  $t_{\text{turn}}$  of these peaks by fitting a Gaussian  $\sim \exp(-2t^2/t_{\text{turn}}^2)$ . This leads to an estimate of the turning angle  $\alpha = t_{\text{turn}} \Omega_{\text{peak}}$ .

A similar procedure was used to estimate the duration of drift periods from the long time series of interflagellar phase difference  $\Delta(t)$ . To reduce noise, and the effect of the short slips, the time derivative  $\Delta'(t)$  of the signal was computed by fitting a second order polynomial to the time series of  $\Delta(t)$  that contain 500 frames (from  $t - 250$  to  $t + 250$ ) and differentiating this fit at time  $t$ . This procedure yields a time series  $\Delta'(t)$  that retains a background signal  $\lesssim 0.5$  rad/s, and occasional large peaks (Fig. S2). We identified peaks to be “large peaks”, when the local maximum of the peak,  $\Delta'_{\text{peak}}$ , was larger than the preceding and succeeding local minima by

1 rad/s. This threshold was verified by checking that the large peaks in  $\Delta'(t)$  correspond to obvious drifts in the interflagellar phase difference. Again, we estimated the duration  $t_{\text{drift}}$  of these peaks by fitting a Gaussian  $\sim \exp(-2t^2/t_{\text{drift}}^2)$ . All slips (jumps of  $\pm 1$  in the time series for  $\Delta(t)$ ) in each experiment were identified and averaged and the time derivative  $\Delta'(t)$  of the averaged signal was then computed. A Gaussian fit  $\sim \exp(-2t^2/t_{\text{slip}}^2)$  to the obtained peak gave then an estimate for the slips duration  $t_{\text{slip}}$ . The “free flight time”  $\tau$  is defined as the time between successive large peaks in  $\Omega(t)$ .

### Diffusion experiment

For each movie the intensity distribution inside the cuvette was integrated along the cuvette width to give the raw signal  $I_{\text{raw}}(x, t)$ , where  $x \in [0, L]$  is the coordinate along the cuvette length, and  $t \in [0, T]$  is the elapsed time from the beginning of the movie. We used  $I_{\text{raw}}(x, 0)$  to estimate the background intensity distribution, which was then subtracted from the raw signal to give the real intensity distribution  $I(x, t)$ . Independent experiments established that this signal is proportional to the local cells’ concentration, at least for concentrations up to  $\sim 2 \times 10^6$  cells/ml. The initial intensity profile is typically localized in the bottom 10% of the cuvette (2 mm, with the peak at 1 mm). During an experiment it spreads upwards, until at time  $T$  it just reaches the upper limit of the region of interest. Given  $l$  such that  $I(l, T) = 0.5 \times \max(I(x, T))$ , we estimated intensity gradients and fluxes at a uniformly spaced set of points for  $x \in [l, L]$  and  $t \in [0, T]$ . The gradients were calculated from a local linear interpolation to the intensity profile. The fluxes were estimated from the time changes in the integrated intensity above the point of interest. The linear relation between measured fluxes and gradients (Fig. 1A) is a clear verification of Fick’s law and allows a direct determination of the diffusion constant for an isolated individual:  $D_{\text{exp}} = (0.68 \pm 0.11) \times 10^{-3} \text{ cm}^2/\text{s}$  (from  $n = 8$  population trials).

From the initial position of the peak, the spread of the intensity distribution at time  $T$ ,

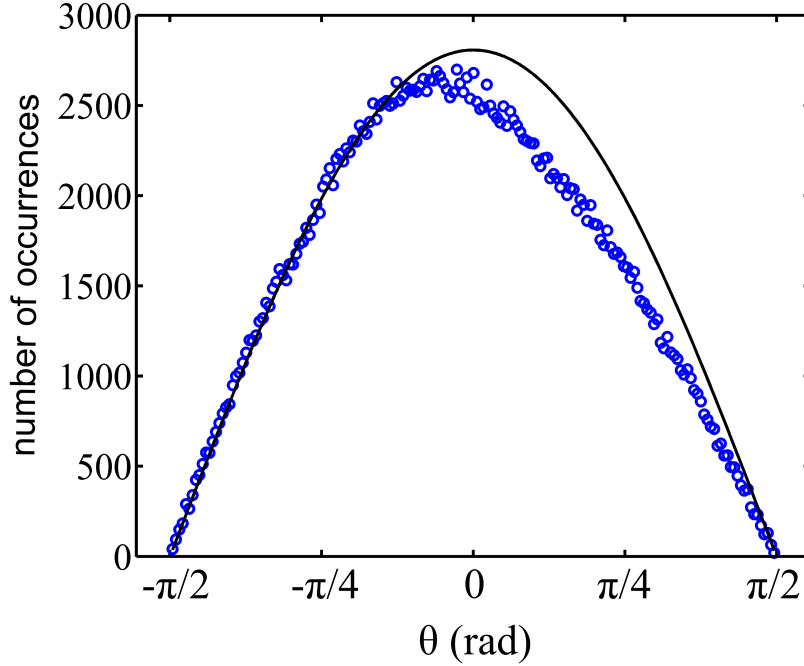


Figure S3: Comparing the distribution of swimming angles (rad) over the horizontal plane from 3D tracks (circles), and the expected distribution for isotropic swimming (solid line) shows a net preference for upward swimming (negative angles).

and the average cell density (measured a posteriori with the cell counter), we can estimate the maximum value of the cell concentration in the selected range ( $x \in [l, L]$  and  $t \in [0, T]$ ). The estimate falls below  $10^6$  cells/ml for all experiments. This concentration is well below that at which close cell-cell encounters may occur more frequently than once per mean flight time, which can be estimated as  $n = 1/(\pi u \tau d^2) \simeq 3 \times 10^6$  cells/ml, where  $u = 100 \mu\text{m/s}$  is the mean swimming speed,  $\tau \simeq 10$  s is the mean free flight time, and  $d = 10 \mu\text{m}$  is the cell's diameter.

*C. reinhardtii* cells often show a slight preference for upward swimming (negative gravitaxis (S23)), which causes a net drift  $v_d$  in the upward direction. This is true also in the present case (Fig. S3). Analysis of the recorded 3D trajectories gives  $v_d = 5 - 10 \mu\text{m/s}$ , in line with previous measurements (S24). This drift will skew our estimate of the diffusion coefficient as

$D_{\text{exp}}/D \simeq (1 + v_d \delta t/\delta x)$ , where  $\delta t$  and  $\delta x$  are the characteristic time and distance at which intensity fluxes and gradients were measured. For  $\delta t \sim 100$  s and  $\delta x \sim 0.5 - 1$  cm we predict that  $D_{\text{exp}}$  will slightly overestimate the diffusion constant:  $D_{\text{exp}} \simeq 1.1 D$ . Furthermore, slight variations in behavior among different individuals in a whole population will result in slightly different diffusivities. The method we use to estimate the population's average diffusion constant will bias the estimate again towards higher values, since the individuals with higher diffusivity will tend to be overrepresented in the analyzed range. This is also a weak effect because, for example, a normally distributed ensemble of diffusion constants with a standard deviation twice the mean (and truncated to non-negative diffusivities), would give an estimated average diffusion constant only 20% higher than the real mean. The real distribution of diffusivities is certainly narrower than this example, and will give an even smaller bias. Taken together, these two effects may contribute to the small discrepancy between the measured and estimated diffusion constants.

## References and Notes

- S1. UTEX is the algal culture collection of the University of Texas at Austin.
- S2. D.L. Kirk and M.M. Kirk, *Dev. Biol.* **96**, 493 (1983).
- S3. O.A. Sineshchenkov, K.-H. Jung, and J.L. Spudich, *Proc. Natl. Acad. Sci. USA* **99**, 8689 (2002).
- S4. P. Lariguet and C. Dunand, *J. Mol. Evol.* **61**, 559 (2005).
- S5. D.B. Weibel, P. Garstecki, D. Ryan, W.R. DiLuzio, M.Mayer, J.E. Seto, and G.M. Whitesides, *Proc. Natl. Acad. Sci. USA* **102**, 11963 (2005).

- S6. K. Drescher, K. Leptos, and R.E. Goldstein, *Rev. Sci. Instrum.* **80**, 014301 (2009).
- S7. P. Hegemann and B. Bruck, *Cell. Mot.* **14**, 501 (1989).
- S8. V.A. Vladimirov, M.S.C. Wu, T.J. Pedley, P.V. Denissenko, and S.G. Zakhidova, *J. Exp. Biol.* **207**, 1203 (2004).
- S9. N.A. Hill and D.-P. Häder, *J. Theor. Biol.* **186**, 503 (1997).
- S10. H.C. Berg, *Adv. Opt. Elect. Microsc.* **7**, 1 (1978).
- S11. U. Ruffer and W. Nultsch, *Cell. Mot.* **18**, 269 (1991).
- S12. C. Brennen and H. Winet, *Ann. Rev. Fluid Mech.* **9**, 339 (1977).
- S13. I. H. Riedel-Kruse, A. Hilfinger, J. Howard, and F. Jülicher, *HFSP J.* **1**, 192 (2007).
- S14. A. Pikovsky, M. Rosenblum, and J. Kurths, *Synchronization. A universal concept in non-linear science* (Cambridge University Press, Cambridge, 2001).
- S15. T. Niedermayer, B. Eckhardt, and P. Lenz, *Chaos* **18**, 037128 (2008).
- S16. P. Hänggi, P. Talkner, and M. Borkovec, *Rev. Mod. Phys.* **62**, 251 (1990).
- S17. P. Reimann, C. van den Broeck, H. Linke, P. Hänggi, J.M. Rubi, and A. Pérez-Madrid, *Phys. Rev. E* **65**, 031104 (2002).
- S18. U. Ruffer and W. Nultsch, *Cell. Mot.* **5**, 251 (1985).
- S19. R. Kamiya and E. Hasegawa, *Exp. Cell Res.* **173**, 299 (1987).
- S20. N. Okita, N. Isogai, M. Hirono, R. Kamiya, and K. Yoshimura, *J. Cell Sci.* **118**, 529 (2005).

S21. U. Ruffer and W. Nultsch, *Cell. Mot.* **15**, 162 (1990).

S22. G.B. Jeffery, *Proc. London Math. Soc.* **22** (14), 327 (1915).

S23. A. M. Roberts, *Biol. Bull.* **210**, 78 (2006).

S24. B. Bean, *J. Protozool.* **24**, 394 (1977).